110th Anniversary: Effect of System Size on Boundary-Driven Contact Charging in Particulate Flows

110th Anniversary: Effect of System Size on Boundary-Driven Contact Charging in Particulate Flows

Jari Kolehmainen,[†] Lise Ceresiat,[‡] Ali Ozel,[†,‡] and Sankaran Sundaresan[*,†]

†*Department of Chemical and Biological Engineering, Princeton University,Princeton, NJ 08542, USA*

‡*School of Engineering and Physical Sciences, Heriot-Watt University, Edinburgh EH14 4AS, UK*

E-mail: sundar@princeton.edu

Abstract

We study wall-induced triboelectrification of particles by analyzing a continuum model for charge transport. We first consider an idealized case of homogeneous distribution of granular materials in a periodic channel and show that the domain-average charge per particle is inversely proportional to channel size. We then perform three-dimensional simulations of fluidized beds in quasi-periodic channels and cylinders by coupling the charge transport equation with two-fluid model for flow. In both cases, the domain-average charge per particle varies inversely with a characteristic size, namely the channel width and the tube diameter, respectively, just as in the idealized case. The effect of tribocharging at the wall on flow becomes rather weak even for channel widths and tube diameters of only one hundred particle diameters. This implies that the effect of tribocharging at the walls in most flow problems will be limited only to a small boundary layer near the walls.

Introduction

Contact charging or triboelectrification is an every day phenomenon where solid surfaces exchange electrostatic charges when undergoing mechanical contact[1]. Even though triboelectrification has been known for a long time, the microscopic mechanism remains under debate[1–3] and many aspects are poorly understood[4–9]. Triboelectrification takes place in systems of very different length scales ranging from small triboelectric generators[10,11] to dust storms[12,13]. Triboelectrification of particles can occur through interactions of particles of different materials[14,15], particles of the same material but different sizes [16] and particle-wall interactions. The present study focuses on monodisperse particles of the same material where particle-wall interaction is the only mechanism for imparting charges to the particles, which could then be transferred between the particles. Using a recently developed model[17], we analyze the wall-induced tribocharging of particles belonging to Geldart group B in gas-particle flows in vertical channels and cylindrical tubes. In particular, we examine the effect of system size on the domain-average charge per particle (henceforth, simply referred to as mean charge) and the impact of tribocharging on the flow behavior.

Sheeting at the walls is known to be a major concern in polyethylene reactors and tribocharging at the walls has been hypothesized as a possible reason for particle adhesion at the walls[18]; it is also suspected that this tribocharging could affect the bed dynamics even in large industrial scale beds[19,20]. Intuitively, one would expect that the importance of wall-induced tribocharging on the bed dynamics would become weaker as the bed becomes larger, as the surface area to volume ratio decreases with increasing bed dimension. However, how the mean charge changes with system size and at what system size the wall-induced charging in monodisperse systems would become too weak to have an effect on bed dynamics are not known. These are addressed in the present study.

Due to the complex nature of triboelectrification, it comes as no surprise that many different mathematical models have been suggested for triboelectrification that are based on widely differing ideas. These ideas include polarization based charging[21–24]; particle electron

surface density limited charging[25]; high and low energy electrons[26]; particle temperature variations as the driving mechanism[27]; and saturation charge density of the surface limited by dielectric breakdown[28]. However, currently the most commonly used computational models for triboelectrification are based on the effective work function concept and contact potential difference between surfaces[29–38]. In these models, the charging tendency of contacting materials are characterized by an effective work function value that dictates the direction and limit of charging. Most of these prior mentioned models[33,36,37,39] have neglected the role of electric field on the charging, which has been shown to be important in a number of experimental studies[9,35,40]. It has been accounted in some more recent studies and shown to be essential for capturing the experimental results[34,41,42]. The triboelectrification model that we base this study is a variant of the effective work function model[34] that takes the effect of electric field into account and has been used successfully in a number of previous studies to predict granular material charging[41–43].

Much of the prior studies have concentrated on how different particles charge in a given flow domain varies with operational conditions[44–51], but charging of the same particles in different vessels has gained less attention. Hence, in this study we probe the effect of vessel size on the electrostatics while keeping the particle properties unchanged. Furthermore, many studies have focused on the saturated charge level and the evolution of the triboelectrification has received less attention[41,52]. In our earlier work[53], we showed that accelerating the rate of charge transfer did not change the total charge of the system significantly, but altered the charge distribution. Hence, the characteristic time associated with charging plays a role at least in determining the distribution of charge inside flow domain.

Many prior studies have also shown how electrostatic charges can alter particle dynamics[18,20,42,49,54–61]. Most commonly observed effect is particles adhering to the wall and formation of wall layers[18,55], but it also can affect bubble interactions in bubbling beds[20,56,57], mixing in bubbling beds[62], and particle elutriation[49,58–60]. In particular, the electrostatic effects on particle dynamics have shown to depend on charge distribution for bubble dynam-

ics[57] and wall fouling[42]. In our previous study[42], we concluded that the charge distribution depended on the rate of charge transfer, which affected the wall particle layer thickness. In another prior study[53], we showed that the extent of charging was affected by the bed dynamics. Hence, the particle dynamics, charge distribution, and rate of charge transfer are all interconnected.

In this article, we aim at studying coupling between fluid-particle dynamics, charging time-scale, and the size of the flow domain. Understanding effect of the system size is important as almost all experimental measurements and analyses of tribocharging have been done in laboratory-scale devices. In practice, tribocharging can occur through (i) contact between particles and the bounding walls and the internals; and (ii) contact between particles of different type. In the present study, we examine through model analysis how the extent of charging driven by particle-wall work function difference changes with sytem size.

We base our analysis on a recently proposed Eulerian-Eulerian (two-fluid) model[17], which is derived from the aforementioned microscopic contact charging model of Laurentie et al.[34]. Very similar charge-transfer model has been also presented by Ray et. al.[63], where they used the model to study triboelectrification in a 2D fluidized bed. Eulerian-Eulerian model allows for a steady-state analysis that is not available in particle-based (Lagrangian) models as the charges on individual particles are changing all the time. We begin by giving a brief overview of the Eulerian-Eulerian model. We then analyze the case of homogeneous distribution of granular materials in a periodic channel that has an analytical solution for charge distribution and show that the mean charge scales inversely with system size, when particle-wall interaction is the only source of tribocharging. We also investigate how well this prediction derived for such a highly simplified system holds for fluidized gas-particle suspensions in small flow geometries. Specifically we simulate fluidization of 250 μm Geldart group B particles in quasi-periodic channels and in cylindrical tubes, and find that the mean charge varies inversely with the characteristic size of flow domain, just as in the idealized example. For the particles considered in the examples, the effect of tribocharging at the

wall on the bed hydrodynamic becomes rather weak even for channels and tubes whose characteristic size is only ~ 100 times the particle diameter. Based on these results, one can assert that the effect of tribocharging in large industrial beds will be limited only to a small boundary layer near the walls.

Mathematical Modeling

Hydrodynamic Model

We present a brief overview of an Eulerian-Eulerian model for monodisperse charged particles. Readers are referred to our recent article[17] for further details. The continuity equation for solid phase is given by:

$$\frac{\partial \alpha_p}{\partial t} + \boldsymbol{\nabla} \cdot (\alpha_p \boldsymbol{u}_p) = 0, \tag{1}$$

where α_p is the solid volume fraction and $\boldsymbol{u}_p$ is the solid phase velocity.

Gas and solid phase momentum equations are given by

$$\rho_g(1-\alpha_p)\left(\frac{\partial \boldsymbol{u}_g}{\partial t} + \boldsymbol{u}_g \cdot \boldsymbol{\nabla}\boldsymbol{u}_g\right) = (1-\alpha_p)\boldsymbol{\nabla}\cdot\boldsymbol{\Sigma}_g + \boldsymbol{\Phi}_d + \rho_g(1-\alpha_p)\boldsymbol{g} \tag{2}$$

$$\rho_p\alpha_p\left(\frac{\partial \boldsymbol{u}_p}{\partial t} + \boldsymbol{u}_p \cdot \boldsymbol{\nabla}\boldsymbol{u}_p\right) = \alpha_p\boldsymbol{\nabla}\cdot\boldsymbol{\Sigma}_g + \boldsymbol{\nabla}\cdot\boldsymbol{\Sigma}_p - \boldsymbol{\Phi}_d + \rho_p\alpha_p\boldsymbol{g} + \frac{\alpha_p Q_p}{V_p}\boldsymbol{E}, \tag{3}$$

where $\Phi_d = \beta(\boldsymbol{u}_g - \boldsymbol{u}_p)$ is the force per unit volume of the mixture exerted on the gas phase by the solid phase, where β is the drag coefficient modeled by Wen and Yu drag[64]; $\boldsymbol{\Sigma}_i$ $(i = g, p)$ is the phase total stress; $\boldsymbol{g}$ is the gravitational acceleration; Q_p is the local-average charge per particle, V_p is the volume of a particle; $\boldsymbol{E}$ is the local electric field. The electric field is computed from the electrical potential ϕ as $\boldsymbol{E} = -\boldsymbol{\nabla}\phi$. The electrical potential depends on the local charge density according to the Gauss law:

$$\varepsilon_0 \nabla^2 \phi = -\frac{\alpha_p Q_p}{V_p}, \tag{4}$$

where ε_0 is the vacuum permittivity. It should be noted that the Eq. (4) neglects polarization effects on the electric field and differs from models that treat the permittivity as a function of the particle volume fraction[20,56,57]. Hence, Eq. (4) is valid for conducting particles or mildly polarizing insulators that do not exhibit significant polarization. Gas and solid phase stresses are decomposed into isotropic and deviatoric parts:

$$\boldsymbol{\Sigma}_i = -(p_i - \mu_{b,i}(\boldsymbol{\nabla}\cdot\boldsymbol{u}_i))\mathbf{I} + \mu_{s,i}\left(\boldsymbol{\nabla}\boldsymbol{u}_i + \boldsymbol{\nabla}\boldsymbol{u}_i^{\mathrm{T}} - \frac{2}{3}(\boldsymbol{\nabla}\cdot\boldsymbol{u}_i)\mathbf{I}\right) \quad \text{where } i = p, g. \tag{5}$$

The bulk viscosity of gas phase $\mu_{b,g}$ is set to zero and the shear viscosity of gas phase $\mu_{s,g}$ is taken to be air viscosity at ambient conditions. The effect of sub-grid scale gas turbulence is not taken into consideration, as its effect is expected to be minimal because of the high particle Stokes number (see Table 1) and the fine grid resolution used in the simulations.

The solid phase pressure is modelled by[65]:

$$p_p = \rho_p\alpha_p\Theta_p\left(1 + 2(1+e_p)g_0(\alpha_p)\alpha_p\right), \tag{6}$$

where e_p is the coefficient of restitution, $g_0(\alpha_p)$ is the radial distribution function at contact[65], Θ_p is the granular temperature. Shear and bulk viscosities are computed according to[66]:

$$\mu_{s,p} = \frac{4}{5}\alpha_p^2\rho_p d_p g_0(1+e_p)\sqrt{\frac{\Theta_p}{\pi}} + \frac{2\frac{5\sqrt{\pi}}{96}\rho_s d_s\sqrt{\Theta_p}}{(1+e_p)g_0}\left[1 + \frac{4}{5}g_0\alpha_p(1+e_p)\right]^2 \tag{7}$$

and

$$\mu_{b,p} = \frac{4}{3}\alpha_p^2\rho_s d_s g_0(1+e_p)\sqrt{\frac{\Theta_p}{\pi}}. \tag{8}$$

The granular temperature is determined by solving a transport equation[65]:

$$\frac{3}{2}[\frac{\partial}{\partial t}(\alpha_p\rho_p\Theta_p) + \boldsymbol{\nabla}\cdot(\alpha_p\rho_p\Theta_p\boldsymbol{u}_p] = \boldsymbol{\Sigma}_p : \nabla\boldsymbol{u}_p + \boldsymbol{\nabla}\cdot(\kappa_p\boldsymbol{\nabla}\Theta_p) - \gamma_p - \beta\left(3\Theta_p - \frac{\beta d_p\|\boldsymbol{u}_g - \boldsymbol{u}_p\|^2}{4\alpha_p\rho_p\sqrt{\pi}\Theta_p}\right) \tag{9}$$

where thermal diffusivity κ_p is given by:

$$\kappa_p = \frac{2}{(1+e_p)g_0}\left[1+\frac{6}{5}(1+e_p)g_0\alpha_p\right]^2\frac{75}{384}\rho_p d_p\sqrt{\pi\Theta_p}+2\alpha_p^2\rho_p d_p g_0(1+e_p)\sqrt{\frac{\Theta_p}{\pi}} \tag{10}$$

and thermal dissipation γ_p is modelled according to Lun et al.[65]:

$$\gamma_p = 12(1-e_p^2)\frac{\alpha_p^2\rho_p g_0}{d_p\sqrt{\pi}}\Theta_p^{3/2}. \tag{11}$$

Although the electrostatic forces could influence the fluctuating motion of the particles, the granular temperature transport equation and the constitutive model for the particle phase stress do not account for them. A general fluctuation energy balance that includes the effect of electrostatics is not available, to the best of our knowledge. The effect of electrostatic forces for monodisperse particles is likely to be more important in the momentum balance (where it is indeed included, see Eq. 3) than in the granular temperature balance[67]. The charge transport equation evolves the distribution of charges, which is needed to compute the electrostatic force; as a result, it is more important than the effect of electrostatic forces on the granular temperature balance.

Charge transfer is modelled by a transport equation derived in a recent article[17]:

$$\frac{\partial}{\partial t}\left(\frac{\alpha_p}{V_p}Q_p\right)+\boldsymbol{\nabla}\cdot\left(\frac{\alpha_p}{V_p}\boldsymbol{u}_p Q_p\right)=-\boldsymbol{\nabla}\cdot(\sigma_q\boldsymbol{E})+\boldsymbol{\nabla}\cdot(\kappa_q\boldsymbol{\nabla}Q_p), \tag{12}$$

where σ_q is the triboelectric conductivity and κ_q is the triboelectric diffusivity, both which are function of particle volume fraction and granular temperature[1]:

$$\sigma_q = \gamma_q 2^{14/5}\frac{5\pi\sqrt{\pi}}{21}\varepsilon_0 g_0(\alpha_p)d_p^3\left(\frac{\alpha_p}{V_p}\right)^2\Gamma\left(\frac{12}{5}\right)r^*\left(\frac{15m_p^*}{16Y^*\sqrt{r^*}}\right)^{2/5}\Theta_p^{9/10} \tag{13}$$

[1]The original expressions given in article[17] had an error in the constant coefficients, which have been corrected in this work.

and

$$\kappa_q = \frac{d_p\sqrt{\Theta_p}}{9\sqrt{\pi}g_0(\alpha_p)V_p} + \gamma_q 2^{14/5}\frac{5\sqrt{\pi}}{21}g_0(\alpha_p)d_p^2\left(\frac{\alpha_p}{V_p}\right)^2\Gamma\left(\frac{12}{5}\right)r^*\left(\frac{15m_p^*}{16Y^*\sqrt{r^*}}\right)^{2/5}\Theta_p^{9/10}, \quad (14)$$

where γ_q is a phenomenological parameter quantifying the rate of charge transfer and $*$ refers to effective quantities; Y^* is the effective Young's modulus; m_p^* is the effective particle mass and r^* is the effective radius. These quantities are defined as:

$$Y^* = \frac{Y}{2(1-\nu^2)}, \quad m_p^* = \frac{m_p}{2}, \quad r^* = \frac{d_p}{4} \quad (15)$$

where ν is the Poisson's ratio. The first term in the triboelectric diffusivity accounts for the diffusive motion of the charged particles, while the second term is due to the charge transfer between particles during particle-particle contact.

Earlier work[53,68] has used the parameter γ_q to adjust the rate of charge transfer. Laurentie et al[34] obtained good agreement between their vibrated bed data and numerical simulations using $\gamma_q = 1$ (this adjustable parameter was not introduced in their study and hence the default value of unity). However, in our recent both vibrated bed[41] and fluidized bed[42] studies, this charging model was found to overestimate the rate of charge transfer. By comparing the experimental and simulation results, it was found that $\gamma_q \approx 1/60$ matched the results better than unity. It should be noted that Laurentie et al.[34] studied polycarbonate and polyamide particles as opposed to studies[41,42], which used polyethylene particles in glass containers. Hence, γ_q appears to be affected by the system of interest. With this in mind, in the present study we have treated γ_q as a model parameter and probed how changing it affected our findings.

The material properties and simulation parameters used in this study are summarized in Table 1.

Table 1: Material properties and simulation parameters. Superscripts refer to a specific case where variables are used; $*$: isothermal homogenous granular medium, †: fluidized particles in a channel, ‡: fluidized gas-particle mixtures in cylindrical tubes.

Material properties and simulation parameters	**Value**
Particle diameter; d_p $[\mu m]$	250
Particle density; ρ_p [kg/m^3]	910
Young's modulus; Y [Pa]	7×10^{10}
Poisson's ratio; ν	0.42
Particle-particle restitution coefficient; e_p	1^*, $0.9^{\dagger,\ddagger}$
Particle-wall restitution coefficient; e_w	1^*, $0.9^{\dagger,\ddagger}$
Gas density; ρ_g $[kg/m^3]$	$1.3^{\dagger,\ddagger}$
Gas viscosity; μ_g $[Pa \cdot s]$	$1.8{\times}10^{-5\dagger,\ddagger}$
Gravitational acceleration; $\lvert\mathbf{g}\rvert$ $[m/s^2]$	$9.81^{\dagger,\ddagger}$
Terminal velocity based on Wen and Yu drag law[64] ; v_t [m/s]	$0.91^{\dagger,\ddagger}$
Particle Reynolds number; $Re_p = \frac{\rho_g \, v_t \, d_p}{\mu_g}$	$16.5^{\dagger,\ddagger}$
Particle Stokes number; $St_p = \frac{1}{18}\frac{\rho_p}{\rho_g} Re_p$	$690^{\dagger,\ddagger}$

Boundary Conditions

Following our earlier work[17], charge at a conducting boundary satisfies the following boundary condition:

$$\sigma_{q,w}\left(\frac{\Delta\varphi}{\delta_c e} - \frac{2Q_p}{\pi\varepsilon_0 d_p^2}\right) + \kappa_q \boldsymbol{n}_w \cdot \boldsymbol{\nabla} Q_p - (\sigma_q - \sigma_{q,w})\, \boldsymbol{E} \cdot \boldsymbol{n}_w = 0, \tag{16}$$

where $\Delta\varphi$ is an effective work function difference between particles and the wall; $e > 0$ is the elementary charge; δ_c is the electron tunneling distance; $\boldsymbol{n}_w$ is the inward normal of the wall (pointing from the wall to the interior domain). Triboelectric conductivity at the wall ($\sigma_{q,w}$) is given by:

$$\sigma_{q,w} = \gamma_q \varepsilon_0 \alpha_p \left(1 + 2(1+e_w)\alpha_p g_0\right) \left(\frac{6\left(\frac{15\, m_p}{16 Y^* \sqrt{r}}\right)^{\frac{2}{5}} \Gamma(\frac{9}{10})}{\sqrt[10]{2}(1+e_w) d_p^2}\right) \Theta^{9/10}, \tag{17}$$

where e_w is the restitution coefficient of wall-particle collisions.

In the simulations of gas-particle suspension, no-slip boundary condition is applied to both phase velocities at the bounding walls; granular temperature and pressure follow a zero

normal gradient boundary condition. Gas velocity is specified at the inlet and it satisfies a zero gradient boundary condition at the outlet.

Isothermal Homogenous Granular Medium

Periodic Channel

Here we consider an idealized problem that allows for an analytical solution so that the effect of scale-up can be exposed easily. Specifically, we neglect the gravitational acceleration and analyze only the granular medium; particle-particle and particle-wall restitution coefficients are set to unity and the effect of the electrostatic force on the particles is taken to be negligible so that the particles are distributed homogeneously in the channel and they maintain a constant granular temperature. In this limiting case, one can obtain an analytical solution for the charge distribution, as outlined below. Under these assumptions, the Eulerian-Eulerian model simplifies to:

$$-\left(\frac{\sigma_q}{\varepsilon_0}\right)\tilde{Q}_p + \left(\frac{V_p \kappa_q}{\alpha_p L^2}\right)\frac{d^2\tilde{Q}_p}{d\tilde{x}^2} = 0, \tag{18}$$

$$\frac{d^2\tilde{\phi}}{d\tilde{x}^2} = -\alpha_p \tilde{Q}_p \tag{19}$$

where $\tilde{x} = x/L$ refers to the dimensionless channel coordinate (normal to the walls), and the channel walls are placed at positions $x = -L/2$ and $x = L/2$. The dimensionless variables are given by

$$\tilde{Q}_p = \frac{Q_p}{q_{eq}}, \tag{20}$$

$$\tilde{\phi} = \left(\frac{\varepsilon_0 V_p}{L^2 q_{eq}}\right)\phi. \tag{21}$$

Here, q_{eq} is the equilibrium charge that is the largest charge attainable by the particles due to work function difference $\Delta\varphi$ and it is computed by:

$$q_{eq} = \frac{\Delta\varphi \pi \epsilon_0 d_p^2}{2\delta_c e}. \tag{22}$$

The nature of the solution to this problem is determined by the ratio of two time scales, one associated with tribocharging, τ_e, and the other representative of charge diffusion, τ_d:

$$\tau_e = \frac{\varepsilon_0}{\sigma_q}, \tag{23}$$

$$\tau_d = \frac{\alpha_p L^2}{V_p \kappa_q}. \tag{24}$$

With introduction of these two time scales, the charge transport equation in the channel becomes:

$$-\tilde{Q}_p + \frac{\tau_e}{\tau_d}\frac{d^2\tilde{Q}_p}{d\tilde{x}^2} = 0. \tag{25}$$

The boundary condition for the electric potential at the wall is simply $\tilde{\phi} = 0$ while for charge it becomes:

$$-(1-\tilde{Q}_p) - 3\alpha_p \left(\frac{L}{d_p}\right)\left(\frac{\tau_{e,w}}{\tau_d}\right)\frac{d\tilde{Q}_p}{d\tilde{x}} + 3\left(\frac{L}{d_p}\right)\left(\frac{\tau_{e,w}}{\tau_e} - 1\right)\tilde{E}_{w,x} = 0. \tag{26}$$

The variation of scaled charge $\tilde{Q}_p$ in the channel is found by solving the above system of equations, and the mean charge readily follows. Our goal is to find how this mean charge changes with the ratio of the system width to the particle diameter, L/d_p. Before describing the results obtained by numerical integration of the above equations using the finite difference method, it is useful to consider first the two limiting cases: (i) $\tau_e << \tau_d$ and (ii) $\tau_d << \tau_e$.

If τ_e is much smaller than τ_d, the diffusion term can be neglected as it will be much smaller than the charge conduction due to the electric field. In this limit, the charge transport equation simplifies to $\tilde{Q}_p = 0$ and hence the electrical potential will be $\tilde{\phi} = 0$. With a

constant electrical potential, the electric field at the wall vanishes and the boundary condition simplifies to $\tilde{Q}_{p,w} = 1$. Hence, in the limit of zero diffusion, particles obtain the equilibrium charge at the wall and particle charge is zero everywhere else. For $0 < \tau_e << \tau_d$, this discontinuous change will be replaced by a thin boundary layer where the scaled charge changes from one at the wall to zero outside the boundary layer. When the boundary layer thickness is very small compared to the system width, the boundary layer at each of the two bounding walls can be analyzed separately and then patched together to get the leading order solution for the average scaled charge on the particles. Such an analysis leads to the following estimate:

$$\langle \tilde{Q}_p \rangle = \frac{2\sqrt{\frac{\tau_e}{\tau_d}}}{1 + 3\alpha_p \sqrt{\frac{\tau_e}{\tau_d}}} \left(\frac{d_p}{L} \right). \tag{27}$$

Thus, we find that the mean charge varies inversely with L/d_p in this limit.

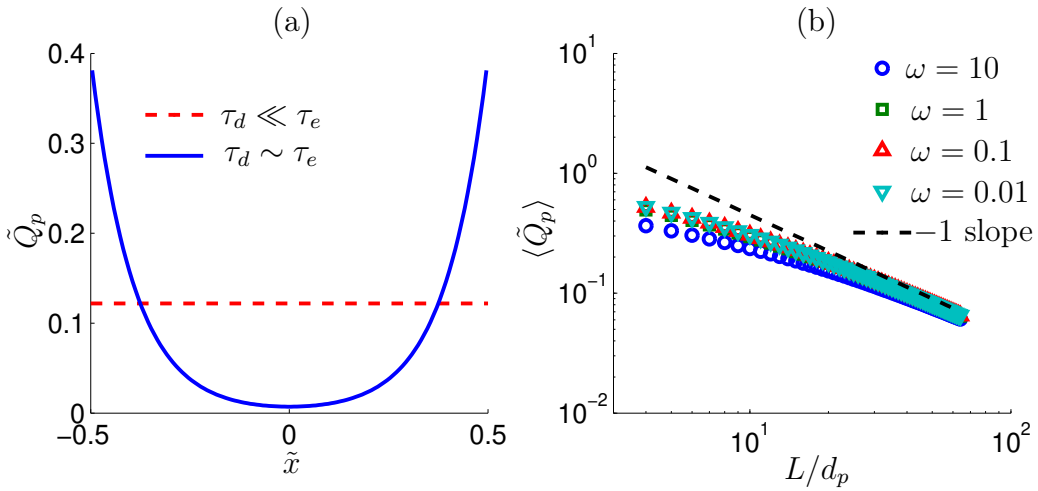

Figure 1: (a) Scaled charge variation in the periodic channel configuration; blue solid line shows the solution for the case where $\tau_d \sim \tau_e$ and red dashed line shows the solution for the case $\tau_d \ll \tau_e$. In both cases, $L = 32d_p$, and $\alpha_p = 0.15$. (b) Domain-average charge per particle in the periodic channel configuration for various ratios of time-scales ($\omega = \tau_d/\tau_e$) plotted against the system width L. Time scales were adjusted by changing the parameter γ_q to keep the ratio the same when system size was changed. Black dashed line shows the -1 slope for reference.

In order to analyze the other extreme where $\omega = \tau_d/\tau_e << 1$, we can invoke the transport equation (see Eq. (25)) and the Gauss law applied to a whole channel to connect the electric

field and the charge gradient at the wall:

$$\tilde{E}_{w,x} = \alpha_p \frac{\tau_e}{\tau_d} \frac{d\tilde{Q}_p}{d\tilde{x}}. \tag{28}$$

Inserting Eq. (28) to Eq. (26), we obtain simpler form of the boundary condition involving only the particle charge:

$$1 - \tilde{Q}_p \pm 3\alpha_p \left(\frac{L}{d_p}\right) \left(\frac{\tau_e}{\tau_d}\right) \frac{d\tilde{Q}_p}{d\tilde{x}} = 0. \tag{29}$$

Then, we invoke a perturbation expansion for the charge

$$\tilde{Q}_p \equiv \sum_{n=0}^{\infty} \omega^n \tilde{Q}_p^{(n)}, \tag{30}$$

where functions $\tilde{Q}_p^{(n)}$ do not depend on the ω. Inserting Eq. (30) into Eq. (25) and solving the order $n = 0$ problem (which also requires analysis of order $n = 1$), we find that

$$\tilde{Q}_p^{(0)}(\tilde{x}) = \frac{1}{1 + \frac{3}{2}\alpha_p \left(\frac{L}{d_p}\right)}. \tag{31}$$

For any practical applications $d_p \ll L$, and $\tilde{Q}_p^{(0)}(\tilde{x}) \propto d_p/L$. Hence, in the limit $\tau_d \ll \tau_e$ the mean charge, corresponding to $\tilde{Q}_p^{(0)}$, will be inversely proportional to the channel width. The profile will be almost flat as opposed to the case $\tau_e \ll \tau_d$. Yet, the mean charge scales with system size in the same manner in both limiting cases. (Both Eqs. (27) and (31) suggest that the natural length scale to use to non-dimensionalize the gap width is d_p. For this reason, we use the particle diameter as the characteristic length.) For intermediate values, the solution lies between these two extreme, which is illustrated in Fig 1a. Fig. 1b shows the mean charge for different channel widths and time-scale ratios resolved by the finite difference method. The figure reveals that the mean charge of the system is fairly independent of the time-scale ratio and begins to follow the inverse relation for channel widths sizes $L > 10d_p$. Note that

the total number of particles increases with the channel width. It is straightforward to use the Gauss law to show that the electric field at the channel walls (in this limit of inverse relation between mean charge and channel width) will be independent of channel width. This implies that the typical magnitudes of electric field experienced by the particles will be independent of channel with. It then follows that the average magnitude of the electrostatic force experienced by the charged particles will decrease roughly linearly with system size, when tribocharging at the walls is the only source of particle charge.

Fluidized Particles in a Channel

In order to investigate if predictions obtained in a highly idealized granular system considered above would hold in more complex flows, we performed Eulerian-Eulerian simulations in a fluidized bed channel. In the channel simulations, inlet and outlet boundary conditions are set on the vertical directions, z-direction. Conducting walls are set in the x-direction (i.e. the walls are in the yz-plane) and periodic boundary conditions were applied in the y-direction. Unlike, the aforementioned idealized cases, we now account for the electrostatic forces in the momentum equations so that the interplay between charging and flow is fully captured. In Geldart classification[69], the particles belong to type B, lying close to the A-B boundary (see Table 1 for particle properties). In each case, the height of bed is settled at $160d_p$ (henceforth referred to as static bed height), and inlet velocity is 50% of the particle terminal velocity (computed by Wen and Yu drag law[64]). It is worth to note that the smaller domain simulations (L/d_p or $D/d_p = 20$ or 30) used grid resolution of $2.5\,d_p$ while in larger domains simulations a grid size of $4\,d_p$ was applied in order to cut down the computational cost. Simulations in smaller domains with $4\,d_p$ grids manifested severe solid volume fraction checker boarding, which was remedied by the finer mesh. This issue was not evident in simulations involving larger domains. Simulations were performed for several different combinations of model parameters, but we show here only a selected subset of the

results.

In our previous study on contact charging in vibrated beds[41], by matching our experimental data on particle charging with Computational Fluid Dynamics-Discrete Element Method (CFD-DEM) simulations and the charging model used in this study[34], we estimated that the effective work function difference between the polyethylene particles and borosilicate glass container is in the $1-2$eV range. This estimate is dependent on the electron tunneling distance, δ_c, assumed. As the effective work function difference increases, the extent of particle charging and the potential influence of electrostatics on flow increase. Results are presented for a particle-wall combination for which the effective work function difference is 2 eV and $\delta_c = 500$ nm. These correspond to the ratio of electrostatic force to gravity: $e/g = q_{eq}^2/(\varepsilon_0 \pi d_p^2 m_p g) \sim 20$ (based on equilibrium charge, defined in Eq. (22)). As noted earlier, q_{eq} is the maximum charge that a particle can acquire in the absence of an externally imposed electric field. This level of charging is possible when an isolated particle is interacting with a conducting wall. The quantity e/g compares the attractive electrostatic force between this particle and a conducting wall that it is in contact with to the weight of this particle. (To put this number in perspective, the inter-particle attractive force between two contacting particles at the Geldart group A/C transition is 10^3 [70].) When many particles are present, as in the problem we are analyzing, the electric field generated by the particles will decrease the charges acquired by the particles. As a result, the domain-average charge per particle in a many particle system, which is referred to as saturation charge, is much smaller than q_{eq} for an isolated particle, as discussed below. Each simulation was performed for 60 s, which was found to be sufficiently long for the system to reach a steady state.

Unless mentioned otherwise, the results presented correspond to the charging rate parameter $\gamma_q = 0.2$. Although $\gamma_q \approx 1/60$ was estimated to be a more realistic choice, running simulations with such small γ_q value is prohibitively expensive at the grid resolutions used in this study. We employed a grid resolution of $2.5 - 4\, d_p$ as the smaller domains require such resolution so that there is an adequate number of grids over the cross section. In order to

ensure that flow structure is resolved to the same level of accuracy, we kept similar grid resolution even when tube radius was increased; this led to a rapid escalation of computational cost. The larger cases took one month to run on a 16-core node for $\gamma_q = 0.2$. If γ_q is reduced to 1/60, the computer time would likely be around one year. In any case, we already know from Figs. 2 and 3 (see below) that if the charging behavior of a system is dominated by charge diffusion at some γ_q value (such as $\gamma_q = 0.2$ in our simulations), it will continue to remain dominated by charge diffusion if γ_q is decreased further and no qualitative changes will be observed. On the other hand, increasing γ_q, enhances charge conduction and could lead to qualitative changes. With this in mind, we also explore the effect of larger γ_q values in our simulation studies.

The typical channel widths considered in the simulations (40 to $160\,d_p$) are very small and would hardly qualify as beds of practical dimensions. We emphasize that the goal of our study is not an analysis of the effect of scale-up on bed hydrodynamics, which is a rich field of study, where a great deal of work has been done on coarse-grained models such as filtered two-fluid models (e.g., see[71]). Instead, we set out to examine how the extent of particle charging due to particle-wall interactions change with system size, so that one can establish the importance (or lack thereof) of wall-induced tribocharging in practical systems. Based on the idealized example discussed above, we anticipate that the mean charge in the bed as well as its effect on the bed dynamics would decrease as the bed becomes larger and larger; however, the typical bed size for which tribocharging driven by the particle-wall interactions could impact the overall flow dynamics is not well understood. Our initial simulations suggested that only in this size range does wall charging have an effect on flow; as a result, we focus on presenting our simulation results in this size range. We did carry out many simulations with different values of model parameters such as effective work function difference at the wall and the charging rate parameter, but we report here only a typical set of results. The implication of these results to tribocharging in larger systems of practically important dimensions will be discussed later.

Results

We compute the domain-average charge per particle, or simply the mean charge, by a Favre averaging over the whole domain as:

$$\langle \tilde{Q}_p \rangle(t) \equiv \frac{\int \alpha_p(\boldsymbol{x}, t) \tilde{Q}_p(\boldsymbol{x}, t) d\boldsymbol{x}}{\int \alpha_p(\boldsymbol{x}, t) d\boldsymbol{x}}. \tag{32}$$

Fig. 2a shows the saturated charge level, which refers to the mean charge in the bed at the statistical steady-state. (The saturated charge different from the equilibrium charge on a particle mentioned earlier, which refers to the maximum charge an isolated particle in contact with a conducting wall can hold. Typically, the saturation charge is much smaller than the equilibrium charge as a result of the effect of self-induced electric field due to all the charged particles in the system.) As can be seen from the figure, mean charge levels in a fluidized channel follow reasonably well the inverse relationship derived for the simpler granular gas problem. We also find that the static bed height had only a very small impact on the mean charge. However, decreasing fluidization velocity lowered the particle charge level. This can be explained by a higher particle volume fraction in the bed, and it is consistent with the trend predicted by Eq. (31) and prior studies[38,45,72,73].

It should be emphasized that the linear fit in Fig. 2a was motivated by the scaling suggested by the idealized example discussed earlier. Departure from this linear relationship is attributed to gas-particle drag and the effect of electrostatics on particle flow, which were not considered in the idealized example, but are included in the simulations. The greater departure seen for the $d_p/L = 1/40$ case is likely due to the meandering flow that was observed for this case. This figure shows that, in spite of the additional complexities arising because of non-uniform flow, the mean charge varies linearly with d_p/L to leading order.

Fig. 2b shows the time evolution of mean charge for various channel widths. The decrease of mean charge with increasing channel width is very apparent. Counter-intuitively, the larger cases reached a saturated state faster. In the context of the present model, this could be

explained by the smaller extent of charging. Particles obtain a much higher charge in the narrower channel cases. It takes s larger number of collisions for a single particle to reach this higher value, and hence longer time.

Fig. 2c show the evolution of the mean charge for various values of γ_q. For γ_q values less or equal to unity, the saturated charge level was affected by the charging-rate only weakly ($\sim 10\%$). This result is consistent with our prior particle scale studies[42,53]. However, when γ_q is increased further to 10, the mean charge level raises to a new plateau (Fig. 2c, inset), which is $\sim 100\%$ larger than it was for $\gamma_q = 0.1$. The mean charge level also becomes coupled with the bed fluctuations that are clearly visible for the $\gamma_q = 10$ case. Thus, when the charging rate is fast and the extent of charging is large enough to start influencing the bed hydrodynamics, the final outcome could depend on the charging rate. This point is further reinforced by Figure 3 (see below) describing the charge and particle distributions.

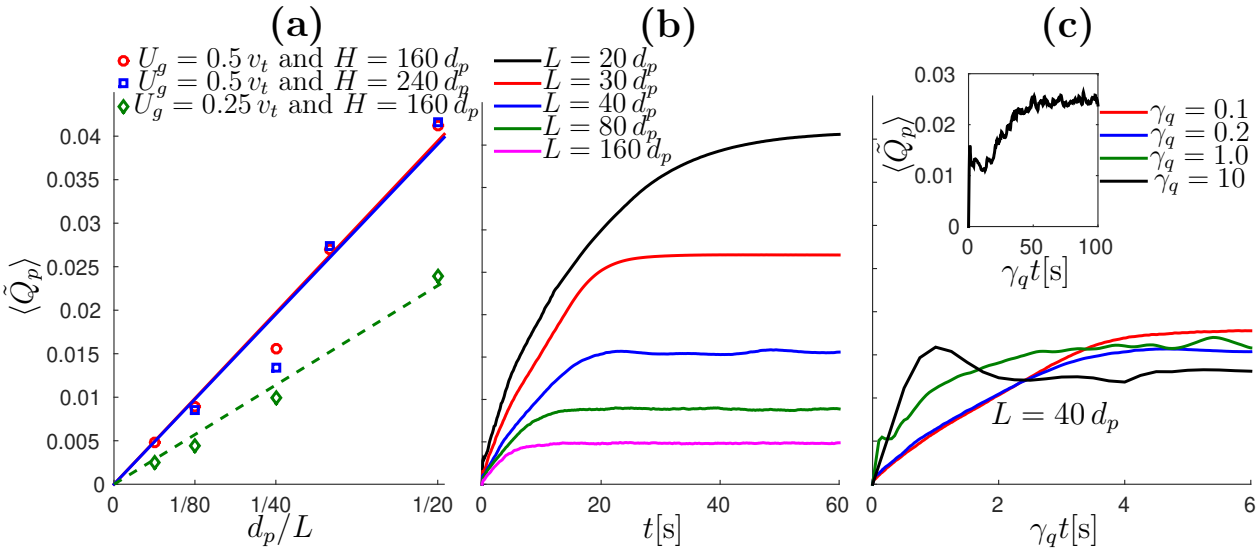

Figure 2: (a) Saturated mean charge level for different channel widths and simulation conditions. Solid and dashed lines show a linear least square fit. (b) Evolution of the domain-average charge per particle with various channel widths ($U_g = 0.5\,v_t$ and $H = 160\,d_p$). (c) Evolution of the domain-average charge per particle for different γ_q values in $L = 40\,d_p$ channel. Inset: Evolution of the domain-average charge per particle with $\gamma_q = 10$. Domain-average charge per particle is scaled by the equilibrium charge: $q_{eq} = 3.456\,\text{nC}$.

Fig. 3a shows profiles of the time-averaged charge in the channel for various channel

widths at $\gamma_q = 0.2$. For smaller channel widths that are diffusion-dominated, the profile is almost flat, consistent with the predictions from the granular gas example discussed earlier. For larger channel widths, the wall charge begins to separate from the interior charge, but the interior remains uniform that can be attributed to the intense mixing due to fluidization.

Fig. 3b shows profiles of the time-averaged charge in $40\,d_p$ wide channel for various γ_q values. As expected, for higher γ_q values the wall charge begins to separate similar to the wider channels. Similarly, the mixing caused by the fluidization keeps the interior profile flat.

Fig. 3c shows snapshots taken after 60 s of fluidization. The rightmost channel shows vigorous slugging of uncharged particles in a $40\,d_p$ wide channel. In the presence of wall-induced tribocharging, most particles in the narrowest channel shown in Fig. 3c are attached to the walls, and the interior is absent of slugging consistent with our prior studies[42,67]. When channel width is increased to $40\,d_p$ the bed switches to a meandering flow, which has also been observed in our prior study[60]. The effect of tribocharging is clearly less severe than that in the $20\,d_p$ channel. Further increase in channel width weakens the effect of tribocharging and the bed begins to slug as in the case of a bed of uncharged particles. Thus, in this example, by the time the channel width becomes $100\,d_p$, the effect of wall-induced tribocharging has become weak and any effect it has is confined to a thin region near the walls. Increasing the channel width further, causes the bed behavior to become more chaotic and form slugs.

Fluidized Gas-Particle Mixtures in Cylindrical Tubes

In this section, we present results for fluidized gas-particle mixtures in small cylindrical tubes in order to expose the inverse scaling of the mean charge with tube diameter. An illustration of the computational domain is given in Fig. 4a. Different from the channel simulations, we now present results for a case where we scale the height of bed settled to a solid volume fraction of 0.5 (referred ad static bed height) along with the tube diameter D. Hence, the

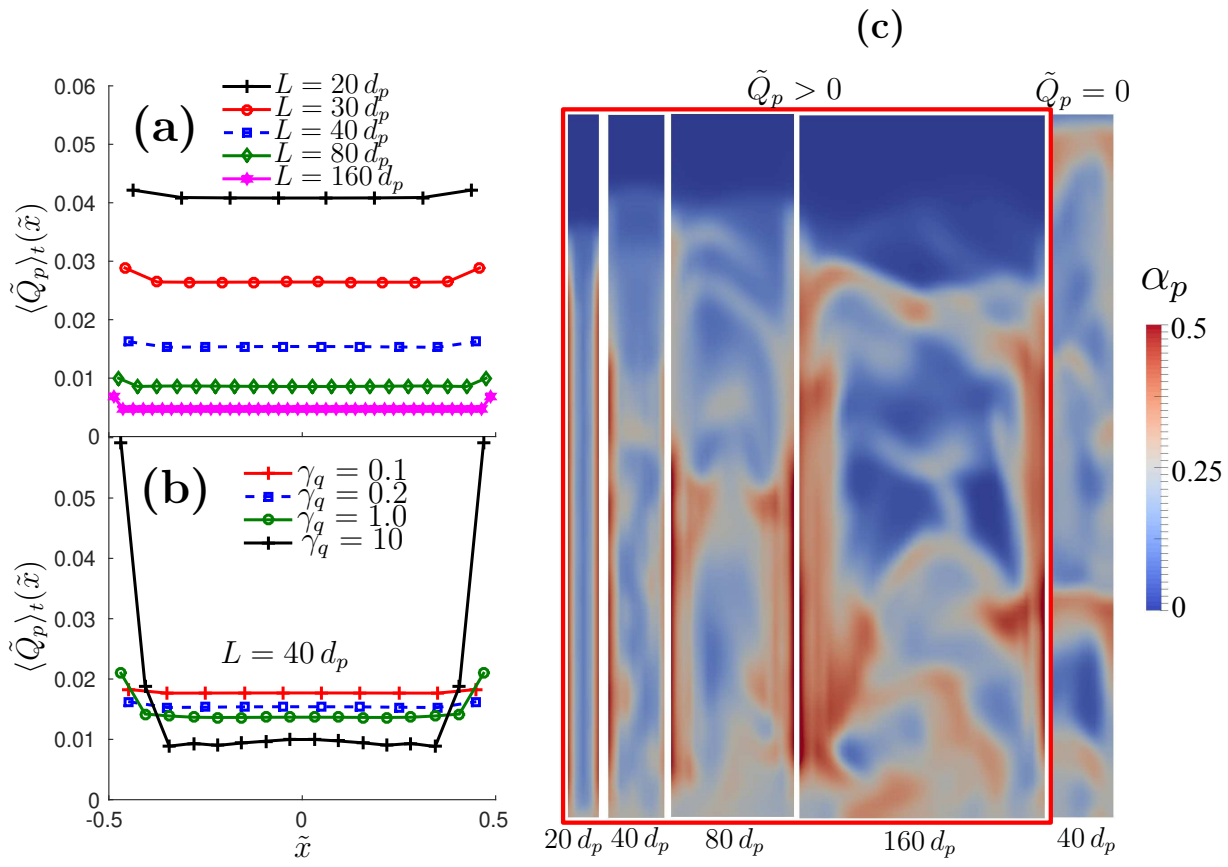

Figure 3: Time-averaged charge profiles as a function of dimensionless x-coordinate ($\tilde{x} = x/L$) for (a) various channel widths with $\gamma_q = 0.2$, and (b) various γ_q values with $L = 40\,d_p$ channel. Channel walls are located in $\tilde{x} = \pm 0.5$ Charge is normalized by the equilibrium charge: $q_{eq} = 3.456\,\text{nC}$. (c) Snapshots taken after 60 s of simulation time for four channel widths: $L = 20\,d_p$, $40\,d_p$, $80\,d_p$, and $160\,d_p$ with $\gamma_q = 0.2$. The rightmost snapshot shows the $L = 40\,d_p$ uncharged channel. Color indicates solid volume fraction and the snapshots shows only the fluidized bed part, which was half of the simulation domain height.

total particle mass now scales with D^3. This scaling of height with diameter is a more natural thing to do. In the channel example, we deliberately kept the static bed height the same so that we can illustrate through the combination of that example and the present one that bed height is not a significant factor in determining the mean charge. Instead, the key length scale is the tube diameter or channel width. The model parameters are the same as in the channel simulations. As in the case of channel simulations, our goal is to examine how the mean charge changes with tube diameter, which is best analyzed by studying really small tubes.

Fig. 4b shows snapshots taken from the center plane of the cylinder. Particles tend to segregate towards the wall because of wall-induced tribocharging. This effect is prominent in small diameter tubes (and narrow channels), where a core-annular flow is clearly observable. As the tube diameter (or channel width) increases, the average particle charge decreases and tribocharging-induced core-annular flow becomes less prominent. The meandering flow pattern observed in narrow channels is not seen in the cylindrical geometry. The interior is homogeneous in both $D = 20\,d_p$ and $D = 40\,d_p$ cases, but the $D = 20\,d_p$ shows the sheet-like wall layer more prominently. These flow patterns have been reported before in literature for uniformly charger particles using both CFD-DEM[67] and Eulerian-Eulerian simulations[19,63]. When the tube diameter is increased, the bed manifests slugging flow, as in the case of uncharged particles. This transition was seen in channel simulations as well.

Time-averaged charge profiles for four different tube diameters are shown in Fig. 4c. The charging behavior of the cylinder is qualitatively similar to the channel, and follows the same inverse (see inset of Fig. 4c) as in the examples discussed earlier.

Discussion

In this study, we have specifically examined how the extent of wall-induced tribocharging of particles changes with system size. By analyzing an idealized case, we first show analytically

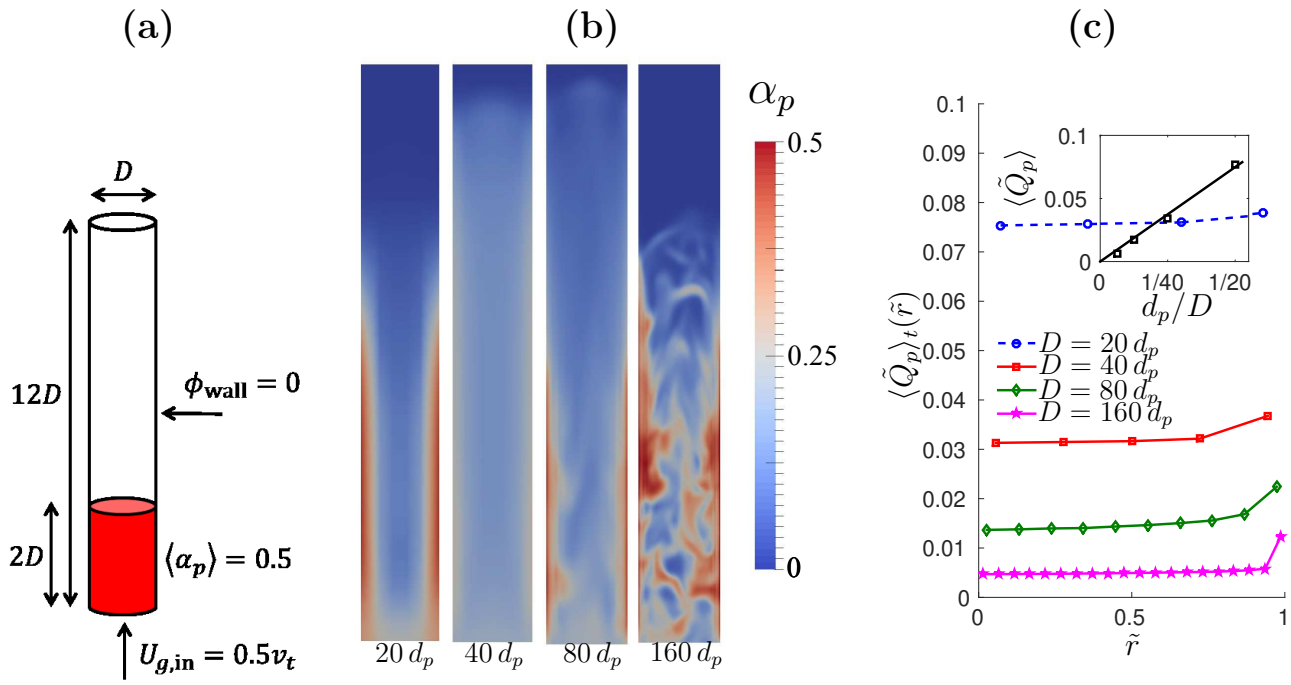

Figure 4: (a) Illustration of the computational domain and initial condition (b) Snapshots taken from the cylinder center plane after 60 s of simulation time for four cylinder bores: $D = 20\,d_p$, $40\,d_p$, $80\,d_p$, and $160\,d_p$. Color indicates solid volume fraction.(c) Time-averaged charge profiles as function of radial component for four different bore sizes considered. The snapshots shows only the fluidized bed part, which was half of the simulation domain height.

that the domain-average charge per particle or namely mean charge manifests an inverse relationship with L/d_p. We then present results from 3D simulations fluidization in channel and cylindrical geometries. Through all these examples, we show that an increase in L/d_p (or equivalently, D/d_p in cylindrical geometries) leads to a decrease in the mean charge on the particles, even though flow behavior varies appreciably among the cases. In other words, the inverse dependence of the mean charge on L/d_p is robust. We further note that scale-up of fluidized beds has been studied extensively in the literature (e.g., see[74–76]). In these studies, L/d_p is not viewed as a meaningful dimensionless group for scaling up (or down) the flow characteristics. Nevertheless, we present our results in dimensionless form in terms of L/d_p, as our inquiry is limited to exploring how the extent of particle charging changes with system size for given particles, wall material and gas superficial velocity. For this limited inquiry, it is therefore reasonable to scale the system size with particle size, for the purpose of presenting the results in dimensionless form.

As shown in the previous sections, our analysis predicts a very rapid decay of the mean charge as the system becomes larger and provides a useful clue as to when this mode of particle charging becomes too weak to be of relevance in devices of practically relevant dimensions. The observed charges are much smaller than the equilibrium charge observed in isolated particles. In our prior experimental study on vibrated beds[41], we observed a rapid decrease in the mean charge when particle mass was increased. This observation supports the theoretical findings of this paper qualitatively. The inverse relationship between extent of charging and the system size is a definite prediction of the model considered in this study. In the channel examples, the static bed height was kept unchanged when varying the channel gap width. Simulations were performed for two different static bed heights (160 and 240 particle diameters). The mean charge for these two different static bed heights are essentially the same, showing clearly that the channel width is the more critical variable. In the cylindrical bed simulations, the ratio of static bed height to bed diameter was held constant when changing the tube diameter. Thus, we have explored both options for static

bed height - keeping it constant or scaling it with D. Both yield similar inverse relationship between average particle charge and system size (L or D). This shows clearly that the bed height is not an important consideration, which can readily be understood when one recognizes that the electric field is predominantly in the lateral direction.

Although the tribocharging process is complex, this inverse trend can also be understood using a simpler argument that the charging extent is determined by the ratio of bed surface area and bed volume. Based on the results presented in this study, one can make the following scaling arguments for wall-induced tribocharging of monodisperse particles with the same material. When one scales up a fluidized bed, the mean charge will be inversely proportional to the bed diameter. At the same time, as the number of particles in the bed per unit height varies quadratically with tube diameter, the total charges in the bed per unit height will increase linearly with bed diameter. The typical range of electric fields generated by these charges will essentially be independent of bed size, but the voltages in the center of the bed (relative to the bounding walls) will increase linearly with system size, which could lead to safety concerns. Concurrently, the influence of the electrostatic force on the bed dynamics will become less and less relevant as the average electrostatic force on a particle will vary inversely with bed diameter. In addition to the scaling relations, the computations described in this paper show that wall-induced tribocharging has no more than a weak effect on bed hydrodynamics when the bed diameter exceeds $100\,d_p$. Such small diameters are irrelevant for fluidized beds, but could be relevant in hopper discharges and flows through draft tubes in small spouted beds[77].

According to the model analyzed in the present study, the influence on wall-induced triboelectric charging in large systems will be confined to a region close to the wall. This, in turn, means that hydrodynamic characteristics, such as bubble shape, in the interior of large beds of practically meaningful dimensions will not be significantly altered by the small level of charging in the bed when particle-wall contact is the only source of tribocharging.

It is also widely accepted that a mixture of particles of different sizes may exhibit bipolar

triboelectric charging[1,4,6,50] and even identical materials may exchange electrostatic charges during contact[1,7,78]. These effects were not incorporated in the Eulerian-Eulerian model analyzed in this study, and it is likely that the inter-particle charge transfer - due to size differences or other reasons - is likely to dominate any wall effects in the interior of large industrial scale vessels. When bipolar charges arise in the bed due to charge transfer between particles of different sizes, they could affect the flow. For example, the small particles could adhere to the oppositely charged larger particles, forming clusters, which in turn would affect the bed dynamics and change the rate of elutriation of the small particles from the bed. It would be interesting to study such complexities introduced by inter-particle charging.

Summary

Flowing particles can pick up electrostatic charges for multiple reasons: (a) particle-wall contact; (b) contact between particles of the same type, but different sizes; and, (c) contact between different types of particles. The latter two types of interactions occur in the interior of the bed and can therefore be expected to be relevant for particle handling devices (such as fluidized beds) of all sizes. In contrast, the importance of particle-wall interactions can intuitively be expected to diminish as one increases the size of the flow domain, as the ratio of the bounding wall surface area to device volume decreases as the device volume increases. In this study, we have examined how the extent of wall-induced tribocharging of monodisperse particles of the same material changes with system by analyzing a continuum model for flow with tribocharging. The principal result from this study is that the domain-average charge per particle varies inversely with the size of the flow domain. We find that the effect of wall-induced charge on flow becomes weak when the system size becomes $100\,d_p$; as a result, the effect of wall-induced tribocharging in fluidized beds will be largely limited to the wall region. It then implies that tribocharging due to particle-particle contact interactions - either because the particles are made of different materials or because there is a size

distribution - is likely to be the principal contributor for effects of tribocharging observed in the interior of large beds. Future studies should expand the Eulerian tribocharging model to polydisperse systems so that the consequences of charging in polydisperse systems could be probed thoroughly.

Acknowledgements

The authors would like to thank ExxonMobil Res. & Eng. Co. for funding this research. Financial assistance for the project through National Science Foundation Grant CBET-1601986 is gratefully acknowledged.

References

(1) Lacks, D.; Mohan, S. Contact electrification of insulating materials. *J. Phys. D: Appl. Phys.* **2011**, *44*, 453001.

(2) McCarty, L. S.; Winkleman, A.; Whitesides, G. M. Ionic electrets: electrostatic charging of surfaces by transferring mobile ions upon contact. *J. Am. Chem. Soc.* **2007**, *129*, 4075.

(3) McCarty, L.; Whitesides, G. Electrostatic charging due to separation of ions at interfaces: Contact electrification of ionic electrets. *Angew. Chem., Int. Ed.* **2008**, *47*, 2188.

(4) Forward, K. M.; Lacks, D. J.; Sankaran, R. M. Charge segregation depends on particle size in triboelectrically charged granular materials. *Phys. Rev. Lett.* **2009**, *102*, 028001.

(5) Soh, S.; Kwok, S. W.; Liu, H.; Whitesides, G. M. Contact de-electrification of electrostatically charged polymers. *J. Am. Chem. Soc.* **2012**, *134*, 20151.

(6) Waitukaitis, S. R.; Lee, V.; Pierson, J. M.; Forman, S. L.; Jaeger, H. M. Size-dependent same-material tribocharging in insulating grains. *Phys. Rev. Lett.* **2014**, *112*, 218001.

(7) Lee, V.; Waitukaitis, S.; Miskin, M.; Jaeger, H. Direct observation of particle interactions and clustering in charged granular streams. *Nat. Phys.* **2015**, *11*, 733.

(8) Schella, A.; Herminghaus, S.; Schröter, M. Influence of humidity on the tribo-electric charging and segregation in shaken granular media. *Soft Matter* **2017**, *13*, 394.

(9) Lee, V.; James, N. M.; Waitukaitis, S. R.; Jaeger, H. M. Collisional charging of individual submillimeter particles: Using ultrasonic levitation to initiate and track charge transfer. *Phys. Rev. Mater.* **2018**, *2*, 035602.

(10) Kim, J.; Chae, S. S.; Han, S. W.; Lee, K. H.; Ki, T. H.; Oh, J. Y.; Lee, J. H.; Kim, W. S.; Jang, W. S.; Baik, H. K. Triboelectric generator based on a moving charged bead. *J. Phys. D: Appl. Phys.* **2016**, *49*, 47LT02.

(11) Wang, Z. L. Catch wave power in floating nets. *Nature* **2017**, *542*, 159.

(12) Renno, N. O.; Wong, A.-S.; Atreya, S. K.; de Pater, I.; Roos-Serote, M. Electrical discharges and broadband radio emission by Martian dust devils and dust storms. *Geophys. Res. Lett.* **2003**, *30*.

(13) Farrell, W.; Smith, P.; Delory, G.; Hillard, G.; Marshall, J.; Catling, D.; Hecht, M.; Tratt, D.; Renno, N.; Desch, M., et al. Electric and magnetic signatures of dust devils from the 2000–2001 MATADOR desert tests. *J. Geophys. Res.: Planets* **2004**, *109*.

(14) Mehrani, P.; Bi, H. T.; Grace, J. R. Electrostatic behavior of different fines added to a Faraday cup fluidized bed. *J. Electrost.* **2007**, *65*, 1.

(15) Zou, H.; Zhang, Y.; Guo, L.; Wang, P.; He, X.; Dai, G.; Zheng, H.; Chen, C.; Wang, A. C.; Xu, C., et al. Quantifying the triboelectric series. *Nat. Commun.* **2019**, *10*, 1427.

(16) Ali, F. S.; Ali, M. A.; Ali, R. A.; Inculet, I. I. Minority charge separation in falling particles with bipolar charge. *J. Electrost.* **1998**, *45*, 139.

(17) Kolehmainen, J.; Ozel, A.; Sundaresan, S. Eulerian modelling of gas–solid flows with triboelectric charging. *J. Fluid Mech.* **2018**, *848*, 340.

(18) Hendrickson, G. Electrostatics and gas phase fluidized bed polymerization reactor wall sheeting. *Chem. Eng. Sci.* **2006**, *61*, 1041–1064.

(19) Rokkam, R. G.; Fox, R. O.; Muhle, M. E. Computational fluid dynamics and electrostatic modeling of polymerization fluidized-bed reactors. *Powder Technol.* **2010**, *203*, 109.

(20) Rokkam, R.; Sowinski, A.; Fox, R.; Mehrani, P.; Muhle, M. Computational and experimental study of electrostatics in gas–solid polymerization fluidized beds. *Chem. Eng. Sci.* **2013**, *92*, 146.

(21) Pähtz, T.; Herrmann, H.; Shinbrot, T. Why do particle clouds generate electric charges? *Nat. Phys.* **2010**, *6*, 364–368.

(22) Siu, T.; Cotton, J.; Mattson, G.; Shinbrot, T. Self-sustaining charging of identical colliding particles. *Phys. Rev. E* **2014**, *89*, 052208.

(23) Yoshimatsu, R.; Araujo, N.; Shinbrot, T.; Herrmann, H. Field driven charging dynamics of a fluidized granular bed. *Soft matter* **2016**, *12*, 6261.

(24) Yoshimatsu, R.; Araújo, N. A. M.; Wurm, G.; Herrmann, H. J.; Shinbrot, T. Self-charging of identical grains in the absence of an external field. *Sci. Rep.* **2017**, *7*.

(25) Duff, N.; Lacks, D. J. Particle dynamics simulations of triboelectric charging in granular insulator systems. *J. Electrost.* **2008**, *66*, 51.

(26) Kok, J.; Lacks, D. Electrification of granular systems of identical insulators. *Phys. Rev. E* **2009**, *79*, 051304.

(27) Gu, Z.; Wei, W.; Su, J.; Yu, C. W. The role of water content in triboelectric charging of wind-blown sand. *Sci. Rep.* **2013**, *3*, 1337.

(28) Korevaar, M.; Padding, J.; Van Der Hoef, M.; Kuipers, J. Integrated DEM-CFD modeling of the contact charging of pneumatically conveyed powders. *Powder Technol.* **2014**, *258*, 144.

(29) Harper, W. Contact and frictional electrification. Ph.D. thesis, Oxford, 1967.

(30) Schein, L. B.; Castle, G. P.; Lacks, D. J. Triboelectrification. *Wiley Encyclopedia of Electrical and Electronics Engineering* **1999**, 1.

(31) Matsuyama, T.; Yamamoto, H. Characterizing the electrostatic charging of polymer particles by impact charging experiments. *Advanced Powder Technol.* **1995**, *6*, 211.

(32) Matsusaka, S.; Maruyama, H.; Matsuyama, T.; Ghadiri, M. Triboelectric charging of powders: A review. *Chem. Eng. Sci.* **2010**, *65*, 5781.

(33) Tanoue, K.; Tanaka, H.; Kitano, H.; Masuda, H. Numerical simulation of triboelectrification of particles in a gas–solids two-phase flow. *Powder Technol.* **2001**, *118*, 121.

(34) Laurentie, J.; Traoré, P.; Dascalescu, L. Discrete element modeling of triboelectric charging of insulating materials in vibrated granular beds. *J. Electrost.* **2013**, *71*, 951.

(35) Mizutani, M.; Yasuda, M.; Matsusaka, S. Advanced characterization of particles triboelectrically charged by a two-stage system with vibrations and external electric fields. *Advanced Powder Technol.* **2015**, *26*, 454.

(36) Grosshans, H.; Papalexandris, M. V. Large Eddy simulation of triboelectric charging in pneumatic powder transport. *Powder Technol.* **2016**, *301*, 1008.

(37) Grosshans, H.; Papalexandris, M. V. Direct numerical simulation of triboelectric charging in particle-laden turbulent channel flows. *J. Fluid Mech.* **2017**, *818*, 465.

(38) Fotovat, F.; Bi, X. T.; Grace, J. R. Electrostatics in gas-solid fluidized beds: a review. *Chem. Eng. Sci.* **2017**, *173*, 303.

(39) Pei, C.; Wu, C.-Y.; Adams, M. DEM-CFD analysis of contact electrification and electrostatic interactions during fluidization. *Powder Technol.* **2016**, *304*, 208.

(40) Zhou, Y. S.; Wang, S.; Yang, Y.; Zhu, G.; Niu, S.; Lin, Z.-H.; Liu, Y.; Wang, Z. L. Manipulating nanoscale contact electrification by an applied electric field. *Nano Lett.* **2014**, *14*, 1567.

(41) Kolehmainen, J.; Sippola, P.; Raitanen, O.; Ozel, A.; Boyce, C. M.; Saarenrinne, P.; Sundaresan, S. Effect of humidity on triboelectric charging in a vertically vibrated granular bed: Experiments and modeling. *Chem. Eng. Sci.* **2017**, *173*, 363.

(42) Sippola, P.; Kolehmainen, J.; Ozel, A.; Liu, X.; Saarenrinne, P.; Sundaresan, S. Experimental and numerical study of wall layer development in a tribocharged fluidized bed. *J. Fluid Mech.* **2018**, *849*, 860.

(43) Naik, S.; Saurabh, S.; Vipul, G.; Bruno, H.; Abramov, Y.; Yu, W.; Chaudhuri, B. A combined experimental and numerical approach to explore tribocharging of pharmaceutical excipients in a hopper chute assembly. *Int. J. Pharm.* **2015**, *491*, 58.

(44) Murtomaa, M.; Rasanen, E.; Rantanen, J.; Bailey, A.; Laine, E.; Mannermaa, J.-P.; Yliruusi, J. Electrostatic measurements on a miniaturized fluidized bed. *J. Electrost.* **2003**, *57*, 91.

(45) Moughrabiah, W. O.; Grace, J. R.; Bi, X. T. Effects of pressure, temperature, and gas velocity on electrostatics in gas-solid fluidized beds. *Ind. Eng. Chem. Res.* **2008**, *48*, 320.

(46) Tiyapiboonchaiya, P.; Gidaspow, D.; Damronglerd, S. Hydrodynamics of electrostatic charge in polypropylene fluidized beds. *Ind. Eng. Chem. Res.* **2012**, *51*, 8661.

(47) Salama, F.; Sowinski, A.; Atieh, K.; Mehrani, P. Investigation of electrostatic charge distribution within the reactor wall fouling and bulk regions of a gas–solid fluidized bed. *J. Electrost.* **2013**, *71*, 21.

(48) Sowinski, A.; Mayne, A.; Mehrani, P. Effect of fluidizing particle size on electrostatic charge generation and reactor wall fouling in gas–solid fluidized beds. *Chem. Eng. Sci.* **2012**, *71*, 552.

(49) Fotovat, F.; Grace, J. R.; Bi, X. T. Particle entrainment from gas-solid fluidized beds: Conductive vs. dielectric fines. *AIChE J.* **2017**, *63*, 1194.

(50) Schella, A.; Weis, S.; Schröter, M. Charging changes contact composition in binary sphere packings. *Phys. Rev. E* **2017**, *95*, 062903.

(51) Song, D.; Mehrani, P. Effect of fluidization pressure on electrostatic charge generation of polyethylene particles. *Ind. Eng. Chem. Res.* **2017**, *56*, 14716.

(52) Liao, C.-C.; Hsiau, S.-S.; Huang, T.-Y. The effect of vibrating conditions on the electrostatic charge in a vertical vibrating granular bed. *Powder Technol.* **2011**, *208*, 1.

(53) Kolehmainen, J.; Ozel, A.; Boyce, C. M.; Sundaresan, S. Triboelectric charging of monodisperse particles in fluidized beds. *AIChE J.* **2017**, *39*.

(54) Al-Adel, M.; Saville, D.; Sundaresan, S. The effect of static electrification on gas-solid flows in vertical risers. *Ind. Eng. Chem. Res.* **2002**, *41*, 6224.

(55) Song, D.; Mehrani, P. Mechanism of particle build-up on gas-solid fluidization column wall due to electrostatic charge generation. *Powder Technol.* **2017**, *316*, 166–170.

(56) Jalalinejad, F.; Bi, X. T.; Grace, J. R. Effect of electrostatic charges on single bubble in gas–solid fluidized beds. *Int. J. Multiphase Flow* **2012**, *44*, 15.

(57) Jalalinejad, F.; Bi, X. T.; Grace, J. R. Effect of electrostatics on interaction of bubble pairs in a fluidized bed. *Advanced Powder Technol.* **2015**, *26*, 329.

(58) Fotovat, F.; Alsmari, T. A.; Grace, J. R.; Bi, X. T. The relationship between fluidized bed electrostatics and entrainment. *Powder Technol.* **2017**, *316*, 157–165.

(59) Yang, Y.; Zi, C.; Huang, Z.; Wang, J.; Lungu, M.; Liao, Z.; Yang, Y.; Su, H. CFD-DEM investigation of particle elutriation with electrostatic effects in gas-solid fluidized beds. *Powder Technol.* **2017**, *308*, 422.

(60) Kolehmainen, J.; Ozel, A.; Gu, Y.; Shinbrot, T.; Sundaresan, S. Effects of polarization on particle-laden flows. *Phys. Rev. Lett.* **2018**, *121*, 124503.

(61) Yao, Y.; Capecelatro, J. Competition between drag and Coulomb interactions in turbulent particle-laden flows using a coupled-fluid–Ewald-summation based approach. *Phys. Rev. Fluids* **2018**, *3*, 034301.

(62) Lim, E. W. C. Mixing behaviors of granular materials in gas fluidized beds with electrostatic effects. *Ind. Eng. Chem. Res.* **2013**, *52*, 15863.

(63) Ray, M.; Chowdhury, F.; Sowinski, A.; Mehrani, P.; Passalacqua, A. An Euler-Euler model for mono-dispersed gas-particle flows incorporating electrostatic charging due to particle-wall and particle-particle collisions. *Chem. Eng. Sci.* **2019**, *197*, 327.

(64) Wen, C.; Yu, Y. H. Mechanics of fluidization. *Chem. Eng. Prog., Symp. Ser.* **1966**, *62*, 100.

(65) Lun, C. K. K.; Savage, S. B.; Jeffrey, D. J.; Chepurniy, N. Kinetic theories for granular flow: Inelastic particles in couette flow and slightly inelastic particles in a general flowfield. *J. Fluid Mech.* **1984**, *140*, 223.

(66) Gidaspow, D. *Multiphase flow and fluidization: continuum and kinetic theory descriptions*; Academic press, 1994.

(67) Kolehmainen, J.; Ozel, A.; Boyce, C. M.; Sundaresan, S. A hybrid approach to computing electrostatic forces in fluidized beds of charged particles. *AIChE J.* **2016**, *62*, 2282.

(68) Pei, C.; Wu, C.; England, D.; Byard, S.; Berchtold, H.; Adams, M. DEM-CFD modeling of particle systems with long-range electrostatic interactions. *AIChE J.* **2015**, *61*, 1792.

(69) Geldart, D. Types of gas fluidization. *Powder Technol.* **1973**, *7*, 285.

(70) Molerus, O. Interpretation of Geldart's type A, B, C and D powders by taking into account interparticle cohesion forces. *Powder Technol.* **1982**, *33*, 81.

(71) Sundaresan, S.; Ozel, A.; Kolehmainen, J. Toward constitutive models for momentum, species, and energy transport in gas–particle flows. *Annu. Rev. Chem. Biomol. Eng.* **2018**, *9*, 61.

(72) Mehrani, P.; Murtomaa, M.; Lacks, D. J. An overview of advances in understanding electrostatic charge buildup in gas-solid fluidized beds. *J. Electrost.* **2017**, *87*, 64.

(73) Ceresiat, L.; Grosshans, H.; Papalexandris, M. V. Powder electrification during pneumatic transport: The role of the particle properties and flow rates. *Journal of Loss Prevention in the Process Industries* **2019**, *58*, 60.

(74) Glicksman, L.; Hyre, M.; Farrell, P. Dynamic similarity in fluidization. *Int. J. Multiphase Flow* **1994**, *20*, 331.

(75) Horio, M.; Nonaka, A.; Sawa, Y.; Muchi, I. A new similarity rule for fluidized bed scale-up. *AIChE J.* **1986**, *32*, 1466.

(76) Song, X.; Bi, H.; Lim, C. J.; Grace, J. R.; Chan, E.; Knapper, B.; McKnight, C. Hydrodynamics of the reactor section in fluid cokers. *Powder Technol.* **2004**, *147*, 126.

(77) Azizaddini, S.; Lin, W.; Dam-Johansen, K. Experimental investigation of a draft tube spouted bed for effects of geometric parameters on operation. AIP Conf. Proc. 2016; p 030043.

(78) Apodaca, M. M.; Wesson, P. J.; Bishop, K. J.; Ratner, M. A.; Grzybowski, B. A. Contact electrification between identical materials. *Angew. Chem.* **2010**, *122*, 958.